

Structural characterisation of MBE grown zinc-blende $\text{Ga}_{1-x}\text{Mn}_x\text{N}/\text{GaAs}(001)$ as a function of Ga flux

Y Han¹, M W Fay¹, P D Brown¹, S V Novikov², K W Edmonds², B L Gallagher²,
R P Champion² and C T Foxon²

¹School of Mechanical, Materials and Manufacturing Engineering &

²School of Physics and Astronomy, University of Nottingham, University Park, Nottingham NG7 2RD, UK

ABSTRACT: $\text{Ga}_{1-x}\text{Mn}_x\text{N}$ films grown on semi-insulating GaAs(001) substrates at 680°C with fixed Mn flux and varied Ga flux demonstrated a transition from zinc-blende/wurtzite mixed phase growth for low Ga flux (N-rich conditions) to zinc-blende single phase growth with surface Ga droplets for high Ga flux (Ga-rich conditions). N-rich conditions were found favourable for Mn incorporation in GaN lattice. α -MnAs inclusions were identified extending into the GaAs buffer layer.

1. INTRODUCTION

III-V ferromagnetic semiconductors are of interest because of their potential application within spintronic device structures (Wolf *et al* 2001). Theoretical prediction of the Curie temperature for various semiconductors (Dietl *et al* 2000) suggests that a T_C value above room temperature is possible for zinc-blende GaN containing 5 at% Mn and a hole concentration of $3.5 \times 10^{20} \text{cm}^{-3}$. In view of the limited solid solubility of Mn in GaN, it becomes necessary to use non equilibrium growth techniques such as plasma-assisted molecular beam epitaxy (PAMBE) to establish appropriate conditions for the growth of uniform $\text{Ga}_{1-x}\text{Mn}_x\text{N}$ alloys. To date, high p-type $\text{Ga}_{1-x}\text{Mn}_x\text{N}$ layers with carrier concentrations exceeding 10^{18}cm^{-3} have been obtained by PAMBE (Novikov *et al* 2004).

Earlier work on the growth of zinc-blende GaN suggests that exact control of the III:V ratio close to the stoichiometric condition allows the production of single phase zinc-blende epitaxial layers, whilst deviation to Ga or N-rich conditions reportedly produces mixed zinc-blende and wurtzite material (Brandt *et al* 1995; Gehler *et al* 1995; Ruvimov *et al* 1997). More recently, various Mn-N or Ga-Mn-N precipitations have been reported for wurtzite GaN epilayers grown on sapphire substrates (e.g. Kuroda *et al* 2003 and Nakayama *et al* 2003).

In this paper, the influence of the Ga:N ratio on the microstructural development of $\text{Ga}_{1-x}\text{Mn}_x\text{N}/\text{GaAs}(001)$ grown by PAMBE is assessed using a variety of complementary analytical techniques.

2. EXPERIMENTAL

Zinc-blende $\text{Ga}_{1-x}\text{Mn}_x\text{N}$ epilayers were grown on semi-insulating (001) oriented GaAs substrates at 680°C by PAMBE. Briefly, a GaAs buffer layer of thickness $\sim 0.15 \mu\text{m}$ was deposited to provide a clean surface for epitaxy. Following initiation of the N plasma, the Mn and N shutters were opened whilst the As shutter was closed. The Mn flux was fixed at a level of 1.0×10^{-8} mbar while the Ga:N ratio was varied by changing the Ga flux from 7.5×10^{-8} mbar to 1.2×10^{-6} mbar. This

corresponded to a transition from N-rich to Ga-rich conditions, with the latter being identified by the development of Ga droplets on the growth surface. An overall chamber pressure of $2\text{-}3 \times 10^{-5}$ mbar was maintained by a flow of N_2 . The growth conditions for the sample set are summarised in Table 1.

The bulk and fine scale defect microstructure of each sample was assessed. A Philips X-pert Diffractometer was initially used to assess the bulk crystal structure of the deposited epilayers. The complementary technique of reflection high energy electron diffraction (RHEED) using a modified Jeol 2000fx transmission electron microscope, with as-grown or HCl etched specimens mounted vertically, immediately beneath the projector lens, was then applied to appraise the sample near surface microstructure. Sample morphology was assessed using an FEI XL30 scanning electron microscope operated at 15-20kV. Samples for TEM investigation across the stoichiometric range were prepared in plan-view and cross-sectional geometries using sequential mechanical polishing and argon ion beam thinning. Samples were assessed using conventional diffraction contrast techniques using Jeol 2000fx and 4000fx instruments and energy dispersive X-ray (EDX) analysis using an Oxford Instruments ISIS system.

Table 1. Growth details of $\text{Ga}_{1-x}\text{Mn}_x\text{N}/\text{GaAs}(001)$ sample set

Sample	Tg / °C	$\text{N}_2 / \times 10^{-5}$ mbar	Ga flux / $\times 10^{-7}$ mbar	Mn flux / $\times 10^{-8}$ mbar	XRD FWHM/°	Ga:N ratio
A	680	2-3	0.75	1	1.15	N-rich
B	680	2-3	1.5	1	0.97	N-rich
C	680	2-3	2.5	1	1.07	N-rich
D	680	2-3	4.6	1	1.17	~1:1 (slightly N-rich)
E	680	2-3	8.0	1	0.95	Ga-rich
F	680	2-3	10	1	0.75	Ga-rich
G	680	2-3	12	1	0.86	Ga-rich

3. RESULTS AND DISCUSSION

The formation of zinc-blende $\text{Ga}_{1-x}\text{Mn}_x\text{N}$ was confirmed by XRD spectra obtained across the sample set. Variation in the full width at half maxima (FWHM) values for the 002 reflection across the stoichiometric range (Table 1) suggests that the layer structural quality becomes optimised for conditions of slightly Ga rich growth. However, no evidence for the presence of second phase wurtzite material was discerned for any of the spectra. As observed using SEM, the sample grown closest to ~1:1 stoichiometric conditions appears specular, indicative of a smooth surface. Samples grown under N-rich conditions appear to exhibit a slightly rougher surface, whilst samples grown under Ga-rich conditions showed increasing amounts of Ga droplets on the sample surface with increasing Ga flux.

RHEED patterns recorded along $\langle 110 \rangle$ projections for samples A, D and G are presented in Fig. 1(a-c). It is noted that clear, sharp spots was only obtained for the Ga-rich samples after removal of surface Ga droplets using boiling HCl. All the samples demonstrated the cubic structure with extra spots and/or streaks indicating varying degrees of mixed phase growth and stacking disorder on inclined $\{111\}$ planes. In particular, a transition from mixed hexagonal/cubic (α/β) phase growth for N-rich conditions to single phase cubic material for Ga-rich conditions was observed (as distinct from the previous indications of XRD).

By way of example, for sample A grown under N-rich conditions, dominant diffraction spots from both cubic and hexagonal material were identified (Fig. 1a). The indexing of Fig. 1a is clarified with reference to the schematic diagram of Fig. 1d which illustrates the orientation relationship between the two phases, with $\langle 110 \rangle_\beta // \langle 11\bar{2}0 \rangle_\alpha$ and $\{111\}_\beta // \{0001\}_\alpha$. It is noted that the extra spots due to the hexagonal phase became faint with increasing Ga flux, disappearing when the Ga:N ratio approached 1:1 stoichiometry (Fig. 1b).

For samples grown under N-rich conditions and ~1:1 stoichiometry, streaks preferentially aligned along one $\langle 111 \rangle$ direction were also observed, indicating the preferential alignment of planar defects (i.e. thin microtwins and stacking faults) inclined to the growth surface on just one set of $\{111\}$ planes (Figs 1 a and b). Similar streaks were observed along both $\langle 111 \rangle$ directions for samples grown under Ga-rich conditions, again attributable to a high density of inclined planar

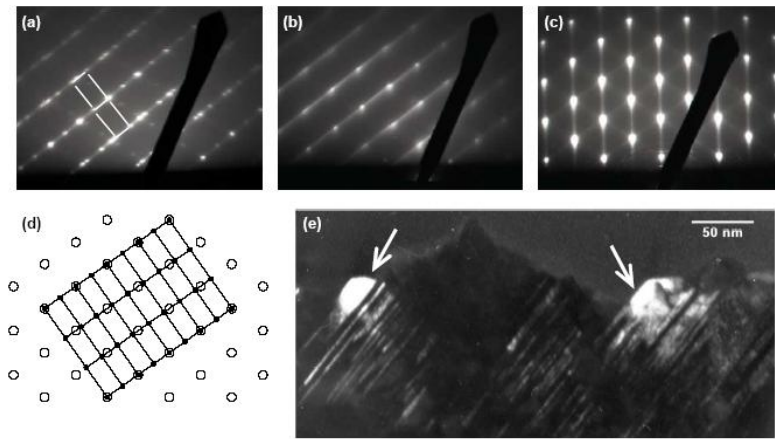


Fig. 1 $\langle 110 \rangle$ RHEED patterns for as-grown $\text{Ga}_{1-x}\text{Mn}_x\text{N}/\text{GaAs}(001)$: (a) sample A, (b) sample D and (c) sample G (HCl etched). (d) Schematic illustration for (a) denoting diffraction spots corresponding to the zinc-blende (open circles) and wurtzite (solid dots) phase; (e) Dark-field, cross-sectional TEM image of the near surface microstructure of sample A suggesting that the wurtzite GaMnN phase arises due to localised small grains at the growth surface (arrowed).

defects (Fig. 1c). It is noted that samples grown under N-rich and nearly 1:1 stoichiometric conditions exhibited strong anisotropy in the distribution of planar defects, being present for just one $\langle 110 \rangle$ sample projection, whilst samples grown under Ga-rich conditions exhibited planar defects for both orthogonal $\langle 110 \rangle$ and $\langle \bar{1}10 \rangle$ sample projections. This variation in the anisotropic distribution of planar defects suggests that this effect is associated with the transition from N-rich to Ga-rich growth, i.e. due to differences in III:V stoichiometry at the growth surface during the process of epilayer nucleation, rather than being due to slight vicinality of the substrate surface. In addition, the presence of streaks perpendicular to the shadow edge of samples grown under Ga-rich conditions (Fig. 1c), following HCl etching, are attributed to patches of relatively smooth surface. More precisely, however, the diffraction effect of streaks perpendicular to the growth surface is attributed to the material that is not perfectly flat, but with slight local misorientations combined with some degree of surface disorder (Cowley 1992).

Overall, the indication from these RHEED patterns together with XRD spectra and SEM observation is that nearly 1:1 stoichiometry (or slightly Ga-rich conditions) correspond to an optimised microstructure.

Fig. 1e shows a centred dark field image formed from a diffraction spot attributed to only wurtzite $\text{Ga}_{1-x}\text{Mn}_x\text{N}$, as distinct from an overlap of spots due to wurtzite $\text{Ga}_{1-x}\text{Mn}_x\text{N}$ and microtwin spots from the zinc-blende $\text{Ga}_{1-x}\text{Mn}_x\text{N}$ located at $1/3\langle 111 \rangle$ positions. This indicates the localisation of small grains of wurtzite $\text{Ga}_{1-x}\text{Mn}_x\text{N}$ at the growth surface. However, the overlap from stacking fault streaks through the objective aperture, due to slight imaging beam convergence, also contributes to this dark field image, partially highlighting the stacking disorder on one set of $\{111\}$ planes. Since selected area diffraction experiments provided no evidence for the presence of wurtzite domains through the bulk of the epilayer and no evidence was found for hexagonal phase material at the epilayer/substrate interfaces, the formation of wurtzite $\text{Ga}_{1-x}\text{Mn}_x\text{N}$ are attributed to a cool down effect at the end of growth whereby a slight change in surface stoichiometry might have occurred under N-rich conditions, allowing small grains of the more stable hexagonal phase to be established. The small volume fraction of these surface hexagonal grains explains why there were not detectable by XRD.

EDX measurements from the epilayers during TEM observation indicated a variation in the Mn content across the sample set, with a relatively uniform Mn content of $\sim 3.3\text{at}\%$ for sample A, peaking at a value of $4 \pm 0.3\%$ for sample D, while the Mn content was below the detectability limit of EDX for samples grown under Ga rich conditions. This is consistent with reports of MBE grown wurtzite $\text{Ga}_{1-x}\text{Mn}_x\text{N}/\text{sapphire}$ which demonstrate that N-rich (and Mn-rich) conditions are required for the successful incorporation of Mn into the crystal lattice (Haider *et al* 2003; Kuroda *et al* 2003), as assessed using EDX and SIMS respectively.

By way of illustration, Fig. 2a presents a dark field image of Sample A, demonstrating the highly faulted nature of the epilayer, and pyramidal precipitates (arrowed) extending into the GaAs buffer layer. EDX measurements confirmed the presence of Mn and As within such inclusions (Fig. 2c), whilst associated selected area electron diffraction patterns (Fig. 2b) confirmed that the inclusions comprised $\alpha\text{-MnAs}$. The indexing of Fig. 2b is clarified with reference to the schematic diagram of Fig. 2d. The orientation relationship here between $\alpha\text{-MnAs}$ and GaAs is given by $\langle 11\bar{2}0 \rangle_{\text{MnAs}} // \langle 110 \rangle_{\text{GaAs}}$ and $\{0001\}_{\text{MnAs}} // \{111\}_{\text{GaAs}}$. It is emphasised that such MnAs inclusions

extending into the buffer layer were identified within all the samples with decreasing size upon transition to Ga-rich growth conditions. No evidence for Ga-Mn-N or Mn-N inclusions was found in these samples.

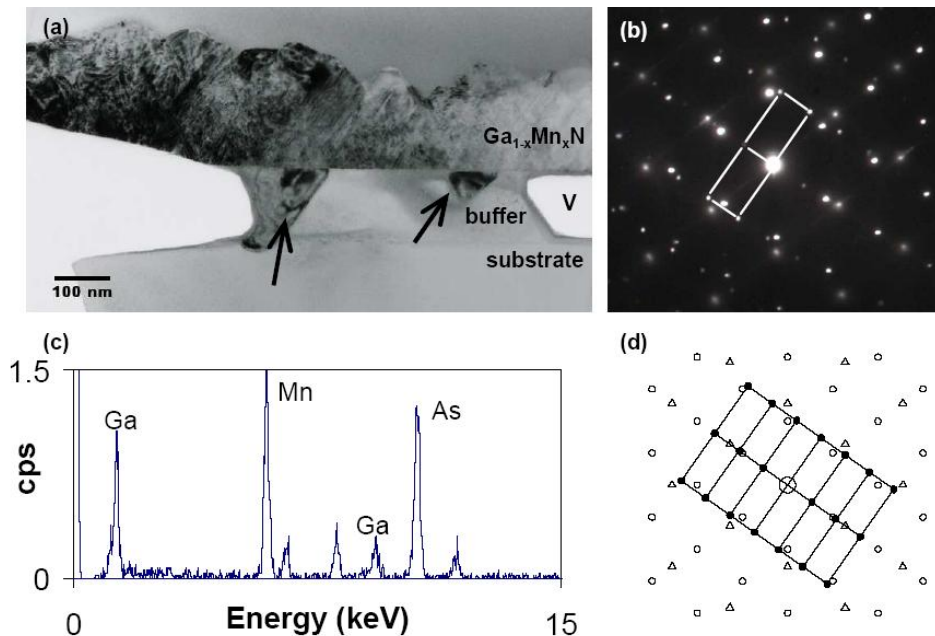


Fig. 2 (a) 002 dark field image of sample A showing α -MnAs inclusions extending into the GaAs buffer layer. (b) Selected area diffraction pattern recorded from the region of an inclusion. (c) EDX spectra demonstrating the inclusions predominantly comprise Mn and As. (d) Schematic illustration denoting diffraction spots due to zinc-blende $\text{Ga}_{1-x}\text{Mn}_x\text{N}$ (open triangles); GaAs (open circles) and α -MnAs (solid dots).

In view of the very different levels of hardness of the epilayer and substrate, it is considered that voids present within the GaAs buffer layer as marked in Fig. 2a arise due to preferential ion beam milling of localised strain centres. However, some co-operative mechanism associated with MnAs precipitate formation during the process of growth might also be implicated in their initial formation.

In summary, N-rich conditions are required for the incorporation of Mn within $\text{Ga}_{1-x}\text{Mn}_x\text{N}$, whilst slightly Ga-rich conditions are associated with optimised structural properties. All samples exhibited MnAs inclusions extending into the GaAs buffer layer, arising from the limited solid solubility of Mn in GaN.

ACKNOWLEDGEMENTS

This work was supported by the EPSRC grants GR/S25630/01 and GR/S81407/01. Y Han would like to thank Keith Dinsdale, Martin Roe, Nicola Weston and Julie Thornhill for their kind technical support.

REFERENCES

- Brandt O, Yang H, Jenichen B, et al. 1995 Phys. Rev. B **52**, R2253
 Cowley J M (1992). Electron Diffraction Techniques. Electron Diffraction: An Introduction. J M Cowley. Oxford, Oxford University Press. **1**
 Dietl T, Ohno H, Matsukura F, et al. 2000 Science **287**(5455), 1019
 Giehler M, Ramsteiner M, Brandt O, et al. 1995 Appl. Phys. Lett. **67**(6), 733
 Haider M B, Constantin C, Al-Brithen H, et al. 2003 J. Appl. Phys. **93**(9), 5274
 Kuroda S, Bellet-Amalric E, Giraud R, et al. 2003 Appl. Phys. Lett. **83**(22), 4580
 Nakayama H, Mashita H, Kulatov E, et al. 2003 J. Magn. Magn. Mater. **258-259**, 323
 Novikov S V, Edmonds K W, Giddings A D, et al. 2004 Semicond. Sci. Technol. **19**, L13
 Ruvimov S, Liliental-Weber Z, Washburn J, et al. 1997 Appl. Phys. Lett. **71**(20), 2931
 Wolf S A, Awschalom D D, Buhrman R A, et al. 2001 Science **294**(5546), 1488